JB 92-14

Parameter Identification of Large Spacecraft Systems Based on Frequency Characteristics"

(with Donald R. Augenstein and Shalom M. Fisher)

10th International Conference on Analysis and Optimization Systems

Sophia-Antipolis, France
June 9-12, 1992

Lecture Notes in Control and Information Sciences 185

R.F. Curtain (Ed.)
A. Bensoussan, J.L. Lions (Honorary Eds.)

Analysis and Optimization of Systems: State and Frequency Domain Approaches for Infinite-Dimensional Systems

Proceedings of the 10th International Conference
Sophia-Antipolis, France, June 9-12, 1992

Springer-Verlag

Parameter Identification of Large Spacecraft Systems Based on Frequency Characteristics

Donald R. Augestein[1] John S. Baras[2] and Shalom M. Fisher[3]

Abstract

In this paper we describe parameter identification for an in-orbit satellite. Actual experimental results are described for the Low Atmospheric Control Experiment (LACE) spacecraft. This is a low earth orbit satellite that was launched into a circular orbit. Its structure consists of a central rigid body or bus with three deployable booms. The first boom is the gravity gradient boom while the second is the retro-reflector boom. We accomplished the identification of the structural modes and damping factors of the spacecraft in orbit. A systems approach was used to analyze the experiment and present identification techniques utilizing the frequency characteristics of the Hankel operator. Frequency domain error bounds and time domain error bounds were considered.

The experiment was performed on a satellite in conjunction with the Naval Research Laboratory. The experiment utilized ground based laser illumination with Doppler shifted returns and identified three of the lowest vibration modes. The accuracy of the methods was extremely good.

1. Introduction

The subject of spacecraft structural parameter identification has gained recent attention. With the development a permanent manned space facility in the near future, the application of sophisticated identification experiments geared to space structures has increasingly become important. Crucial applications of parameter identification of large spacecraft structures are in monitoring structural health and control/structure interactions. Structural identification of the spacecraft in its "true" environment will provide confidence in analytical models and hopefully point to areas where more research is needed. Identification can be used to monitor spacecraft health over its life and analyze trends in performance. Finally, in-flight modeling is a major step toward the goal of real-time adaptive attitude contol and stabilization.

Space structures composed of large solar wings and truss structural elements are typically constructed with fiberglass or graphite composite material. These components are susceptible to large flexible motion. This motion may be driven by solar wind, atmospheric drag, thermal distortion or interaction with the spacecraft's main body. Rigid body dynamics, system vibratory motion, and solar tracking actuators transfer forces to the solar wings at the wing/bus interface thus exciting the wings' vibration.

Because these new space materials have low damping factors, control forces begin to interact with the structural modes. Stiffness requirements for structural rigidity

---

[1] The author was with the Systems Research Center, University of Maryland, he is now with MPR Associates Inc., Washington D.C.

[2] Electrical Engineering Department and Systems Research Center, University of Maryland, College Park, MD 20742

[3] Naval Research Laboratory, Washington D.C.

contribute to the low internal damping. The combination of large elements and low damping creates new design challenges as the spacecraft lowest vibration frequencies begin to extend down into lower frequencies. Because of the low damping factors, all control signals or input forces are required not to generate signals with frequency components near these vibrational modes. Any dynamic motion that does generate forces near these modes may excite large vibrational motion. This resonant motion may present an operational nuisance, but insome cases, it could become disastrous. Unfortunately, as the scale of deployed structures get larger, the lower modal frequencies may begin to seriously limit the actuator operating range. Additionally, actuators that provide incremental pulses (such as stepper motors and thrusters) have signal spectrums which are broad and may excite the structural modes.

While structural analysis can predict modal frequencies with some degree of confidence, the structure configuration over a space structures lifecycle will not be constant. Normal reconfiguration requirements, mechanism decay and failure, and changes in structural properties will create complex structural configurations that may be increasingly hard to model, especially as unknown elements creep into the model formulation. Therefore, there exists a need to independently verify and identify structural behavior.

Recent tests have been done by the US Air Force that tested structural modes on a boom while in the zero-gravity environment of the hold of an airplane in a parabolic dive. More importantly, a complete deployable solar array experiment was performed in the hold of the space shuttle in 1985 (SAFE). The SAFE experiment used attached accelerometers attached at the end of the array. Its excitation force was provided by pulsing the space shuttle's thrusters. While successful, the advantage of this experiment is that the sensing is done remotely and test equipment is not added to the test hardware. Likewise, the spacecraft is in itstrue environment. Finally, this experiment accomplished goals utilizing simple low cost hardware.

1.1. Overview

The following sections will describe the analysis performed for this experiment. Section 2 provides a description of the spacecraft and the details of the data collection. Section 3 details the structural modeling done to provide the baseline values for comparison and describes the algorithmic approach used in the parametric identification. Section 4 explains the experimental results. Section 5 provides an interpretation of the results.

2. Experiment Description

The experiment is to measure vibration of the complete spacecraft structure and calculate the system modal frequencies and damping factors.

2.1. Spacecraft Configuration

The experiment was designed for the Low Power Atmospheric Control Experiment (LACE) spacecraft. It is a low earth orbit satellite that was launched on February 14, 1990 into a 540 km altitude circular orbit of 43° inclination orbit. The LACE spacecraft structure is composed of a central rigid body or bus with three deployable booms (See Figure 1). The bus carries the mission primary sensors and experiments, all supporting telemetry/command modules, attitude and control subsystem and the solar panels.

Each of the deployed booms has a different mission function. The first boom is the gravity gradient boom and is oriented directly away from the earth. It has an electro-magnetic energy dissipating unit located at the tip. The energy dissipation unit is part of a passive attitude stabilization system that dumps destabilizing dynamic energy using the earth's magnetic fields.

The second boom is the retro-reflector boom and is deployed in the direction of the spacecraft velocity vector. The retro-reflector boom tip has a laser reflector unit mounted on it. These reflectors that are part of the primary SDIO spacecraft mission. Amongst these reflectors is a germanium reflector (approximately 1 inch diameter) that is dedicated to this structural dynamics experiment.

The third boom is the balance boom and is oriented 180 degrees from the retro-reflector boom. The balance boom has a strictly passive role of counteracting the rigid body dynamics due to the retro-reflector boom. The rigid body and the balance boom also have germanium reflectors mounted upon them.

The spacecraft booms are both deployable and retractable. The deployed length varies from 0 feet up to 150 feet. The booms' continuous longerons and stiff cross elements are constructed of light weight composite fiberglass/epoxy material. Given that the boom lengths are variable, the system vibration modes are variable as well and are a function of the deployed length . The booms' undeployed portion remains elastically coiled in the deploying canister mounted to the main spacecraft body. Additionally, the deploying canister has an elastic compliance. This compliance is incorporated in the vibration analysis, see Table 1. The rigid central body has a mass of 1177 kilograms with moments and products of inertia listed in Table 2. These properties were experimentally measured. The tip masses on each boom are listed in Table 3.

Table 1: Boom Structural Properties

density unit length kg/m	bending stiffness (EI) N-m^2	torsional stiffness (GJ) N-m^2	Rotating Inertia I_o unit/length N/sec^2	boom canister compliance N/radian
0.291	$\approx 1.55 \times 10^4$	631	2	1.695×10^4

Table 2: LACE Bus Inertial Properties

Inertia	$kg - m^2$
I_{xx}	1448.7
I_{yy}	1426.4
I_{zz}	1026.2
I_{xy}	3.61
I_{xz}	19.98
I_{yz}	14.86

Table 3: LACE Boom tip masses

boom	kg
Gravity	90.7
Retro-reflector	15.9
Balance	15.9

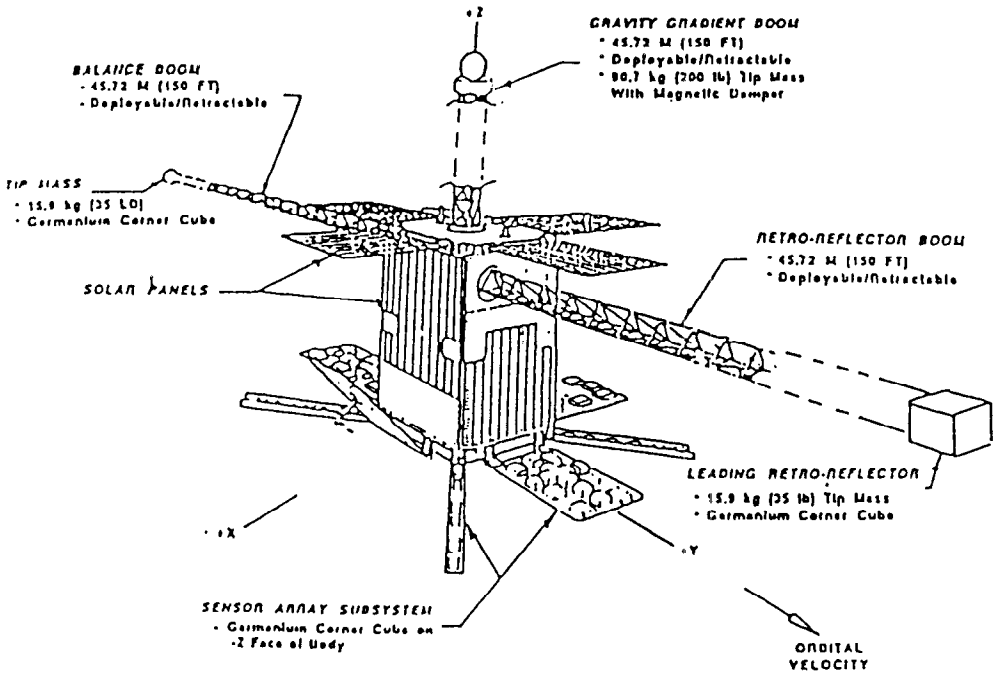

3. Experiment Design

The vibrations are generated by the retraction of a retro-reflector boom from 24.384m (80 ft) to 4.572m (15 ft). This type of excitation is due to two factors. The first is the nonlinear coupling of elastic strains of the boom in its canister. The second is due to the lead tip mass being offset from the axis of the boom. This offset creates a moment at the boom tip which excites vibration. While the excitation forces involved are nonlinear, it should be mentioned that the resulting low level vibration will be within the linear range.

Sampling the vibrations was done remotely. Because the LACE spacecraft does not have telemetered data which can directly indicate the presence of vibratory motion, the measurements were taken indirectly or using remote laser sensing. This technique uses a ground based laser to illuminate the germanium mirrors located on the spacecraft bus and booms. A reflected laser signal will have a Doppler shift due to the relative motion of the spacecraft with respect to the laser source. The Doppler shift from each of the illuminated mirrors is then used to calculate this relative motion.

The laser radar operates at a peak transmit power of 800 watts, with a nominal pulse duration of 3.4 ms, and sampling at 1.2 MHz. The Doppler resolution is about 294 Hz, giving a nominal velocity resolution of 1.8 mm/sec.

Each pulse is sampled 4080 times in-phase and in-quadrature (1.25 Mhz sample rate). The frequency components of the Fourier transform of the complex data set is analyzed to detect Doppler shifts in the return spectrum. The Doppler shifts of each return source is calculated from the sampled power spectrum.

In addition to the vibration motion, the Doppler shift will include the rigid body motion of the satellite's orbital motion. Considering that observation windows are time limited, elimination of this rigid body component is necessary in order to resolve the lowest vibration frequency mode [7].

4. Spacecraft Models

The reference values for the identification results are the modal frequencies calculated from the structural characteristics of the spacecraft. The modal analysis is performed using two techniques. The first technique is finite element modeling (FEM), and the second technique is a continuum approach through a partial differential equation model (PDE). The LACE geometry modeling lends itself to straightforward PDE solution. Thus formulated, the solution of the PDE provides a quick and accurate solution. FEM also provides convenient three dimensional modeling, and its results will converge to PDE solutions only as the number of nodes becomes large. For this experiment, both PDE solutions and FEM solutions were used.

4.1. Euler Beam Model

The basic structural model used was the Euler beam. The Euler beam is the traditional choice because it is a linear model. More complicated models may provide higher "accuracy", however they introduce nonlinear components. These nonlinear components obscure the definition of modal frequency and damping.

The PDE model used to describe the flexible motion of the beam through any axis is as follows:

$$\rho \frac{\partial^2 w(z,t)}{\partial t^2} + EI \frac{\partial^4 w(z,t)}{\partial z^4} = 0 \tag{1}$$

This equation assumes the material stiffness EI and mass per unit length ρ are uniform along the beam. The values for EI and ρ used in this equation are the same as those in Table 1. The solution is calculated using the Laplace transform on the time variable in the equation. Thus, Equation (1) becomes:

$$\frac{\partial^4 \hat{w}(z,s)}{\partial z^4} + \frac{s^2 \rho}{EI} \hat{w}(z,s) = 0 \tag{2}$$

The solution to (2) is:

$$\hat{w}(z,s) = A_1 cos\lambda z + A_2 sin\lambda z + A_3 cosh\lambda z + A_4 sinh\lambda z \tag{3}$$

$$\lambda = (\frac{s^2 \rho}{EI})^{\frac{1}{4}} \tag{4}$$

Likewise, the torsional partial differential equation is described by:

$$I_o \frac{\partial^2 \theta(z,t)}{\partial t^2} + GJ \frac{\partial^2 \theta(z,t)}{\partial z^2} = 0 \tag{5}$$

This equation assumes the torsional stiffness GJ and rotating mass inertia per unit lenghtI_o are constant along the beam. The values for GJ and I_o used in this equation

are the same as those in Table 1. The solution is calculated by using the Laplace transform on the time variable in the equation. The equation (5) becomes:

$$\frac{\partial^2 \hat{\theta}(z,s)}{\partial z^2} + \frac{s^2 I_o}{GJ}\hat{\theta}(z,s) = 0 \tag{6}$$

The solution to (6) is shown to be

$$\hat{\theta}(z,s) = A_1 cos\beta z + A_2 sin\beta z \tag{7}$$

$$\beta = (\frac{s^2 I_o}{GJ})^{\frac{1}{2}} \tag{8}$$

Using equation (4) and the boom's boundary conditions, the values of the coefficients A_i are computed.

4.2. Modeled Modal Frequencies

Using the model of the previous section, the modal properties of the LACE spacecraft were determined. The spacecraft boom length configuration analyzed was the same as the spacecraft's at the time of the experiment (retro-reflector boom at 15ft, gravity-gradient boom at 150ft, and the balance boom at 150ft).

The projection of the boom tip velocity onto the earth observer's line of sight is normal to all vibration except the pitch plane. Thus, the pitch modes are the only modes that are detectable. In Table 4 the pitch modes below one Hertz are listed. Additionally, Table 4 lists the relative magnitude of displacement experienced at the lead tip for each mode. Relative displacement is the ratio of tip deflection to peak deflection. This ratio gives some insight to which modes are most likely to be detected with the ground based laser. Displacement ratios which exhibit large motions at the modal frequency are more likely to be detected. However, it should be noted that there was no guarantee any particular mode would be excited. This is due to the lack of control of the excitation mechanism. It should also be noted that the vibration mode at .7567 Hz is primarily due to the modeled spring compliance of the boom canister. Changing the boundary condition at the spacecraft to a fixed clamp changes this mode. As the modal frequencies get higher, the displacement ratios get larger. This suggests that if the system higher modes could be excited, then they could be easily detected. Unfortunately, the low energy excitation force used in this experiment cannot be expected to generate the higher modes.

PDE hz	FEM hz	Displacement Ratio
.01908	.01906	0.0242
.1298	.12981	0.0063
.2581	.25782	0.0284
.3238	.32333	0.0565
.7567	.74952	0.4669
.8217	.81880	0.1068

Table 4: LACE System Pitch vibration modes below 1 Hertz

4.3. Identification Techniques

Since the form of the excitation or driving function cannot be accurately modeled, the analysis is limited to post-excitation free-decay measurements. Additionally, the observable measurement windows available for laser reflections are extremely limited in time and maybe corrupted by noise. Given these limitations, the identification analysis must be robust in the presence of significant noise and must converge to a model given only a small window of measurements. Analysis has shown that identification using the frequency characteristics of the Hankel operator is the best suited for this experiment.

The system modeling duplicates the structural internal dynamics with an impulse response model. The identification utilizes linear system realization theory which provides error bounds on the model's performance. The performance criteria that is considered is the frequency domain L_∞ norm. The Hankel operator algorithms utilized were the eigensystem realization algorithm (ERA) suggested by Juang *et al* [5] and the minimum model error (MME) suggested by Mook *et al* [1].

4.3.1. Model Reduction Algorithm

The Hankel operator approach assumes that the system response sampled is produced by a linear system's impulse response. With a single input multi-output (SIMO) system (A, B, C) assumed, the discrete system impulse response is described by:

$$Y(k) = CA^{k-1}B$$

If the response is considered a free-decay from an initial condition $x(0)$ the response will be as follows:

$$Y(k) = CA^{k-1}x(0)$$

For the free-decay case of our experiment, the initial condition $x(0)$ will be equated with the input matrix B.

The matrix $H(k)$ is defined to be the Hankel operator time shifted by k time units.

$$H(k) = \begin{bmatrix} Y(k) & Y(k+1) & \dots & Y(k+n) & \dots \\ Y(k+1) & Y(k+2) & \dots & Y(k+n+1) & \dots \\ \vdots & \vdots & & \vdots & \dots \end{bmatrix} \tag{9}$$

It was shown that the zero delayed Hankel operator $H(0)$ has a left-pseudo inverse [5]:

$$H(0)^{\#} = (H(0)^T H(0))^{-1} H(0) \tag{10}$$

The zero delayed Hankel operator has a singular value decomposition:

$$H(0) = U\Sigma V^T \tag{11}$$

$$H(0)^{\#} = V\Sigma^{-1}U^T \tag{12}$$

Using equation (10), the realization (A, B, C) is constructed from the Hankel operator as follows (See Ref [5]).

$$Y(k+1) = E_p^T C A^k B E_m \tag{13}$$

$$= E_p^T H(0) V (\Sigma^{-1} U^T H(1) V)^k \Sigma^{-1} U H(0) E_m \tag{14}$$

$$= E_p^T U \Sigma^{(1/2)} (\Sigma^{(-1/2)} U^T H(1) V \Sigma^{(-1/2)})^k \Sigma^{(1/2)} V^T E_m \tag{15}$$

$E_p^T = [I_p, 0, 0, \cdots,]^T$ and $E_m^T = [1, 0, 0, \cdots,]^T$. The full order realization is constructed with $A = \Sigma^{-1} U^T H(1) V$, $B = \Sigma^{(1/2)} V^T E_m$, and $C = E_p^T U \Sigma^{(1/2)}$. A realization that reduces order in a balanced sense only selects the "large" singular values of the Hankel operator in the construction. Letting $\Sigma_k = diag(\sigma_1, \cdots, \sigma_k)$ representing the k^{th} largest singular values and using matrices U_k and V_k that select the first k columns of U and V, the construction becomes:

$$A = \Sigma_k^{(-1/2)} U_k^T H(1) V_k \Sigma_k^{(-1/2)}$$

$$B = \Sigma_k^{(1/2)} V_k^T E_m$$

$$C = E_p^T U_k \Sigma_k^{(1/2)}$$

It was proven independently by Glover(1984) and Enns [3] using optimal Hankel norm approximations that L_∞ norm of the difference between the n^{th} order true system $G_n(s)$ and the internally balanced truncated k^{th} order model $\hat{G}_k(s)$ has the following bound.

$$\|G(s)_n - \hat{G}_k(s)\|_\infty = \sup_{w \in (-\infty, \infty)} |G_n(jw) - \hat{G}_k(jw)| \leq 2 \sum_{i=k+1}^{n} \sigma_i \tag{16}$$

If the realization (A, B, C) was constructed from noisy Markov parameters, and if an estimate of the noise variance exists, then a comparison of the L_∞ bound and the noise power spectrum is useful. Given a noise power spectrum:

$$\Phi_{noise}(w) = \sum_{-\infty}^{\infty} R_{noise}(\tau) e^{-irw}$$

if the L_∞ bound satisfies:

$$2 \sum_{i=k+1}^{n} \sigma_i \approx \sup_w |\Phi_{noise}(w)|$$

then the effects of the truncation is limited to the removal of modes that model the noise contributions.

4.4. Measuring the distance between truncated systems and infinite systems

Curtain *et al* [6] quantified the effects of truncating the infinite Hankel operator matrix in equation 9 to a finite order matrix. Let Γ_n represent the n^{th} order approximate to the complete Hankel operator Γ. Of interest is the size of appropriate norms on the difference between the truncated and infinite operators $\|\Gamma - \Gamma_n\|$. In order to measure the effects of truncating an infinite Hankel operator Curtain *et al* showed that if the

system impulse response $h(t) \in L_1 \cap L_2$ and the Hankel operator was nuclear, then the truncation of the Hankel operator will converge to the true Hankel operator as the order n gets large.

These intuitive conclusions for a stable system also come with error bounds on performance. This error bound is similar to the one for balanced order truncations. The bound is as follows:

$$\|G - G_n\|_\infty \leq 2 \sum_{i>n} \sigma_i$$

Where G and G_n are the transfer functions associated with the respective Hankel operators. Additionally, there exist performance bounds on the L_1 and L_2 norms on the difference between the truncated and infinite impulse responses.

Nuclearity is dependent on the system under study. It was shown by de Vries [2] that a system constructed via the Laplace transform of a partial differential equation model of a deployed spacecraft essentially equivalent to the LACE spacecraft is in fact nuclear. A necessary assumption is that the booms have viscous damping. This assumption is quite reasonable since the structural damping factor tested on ground was greater than 1 percent. Additionally, any damped structural system is definitely an element of L_1. Thus, the assumption of nuclearity is reasonable.

5. Analysis of Experiment with LACE spacecraft

The experiment yielded four observations windows. Of these windows, only two windows observed the Doppler returns while the spacecraft was in free-decay vibration, days 91008 and 91010. Currently, these two sample periods are the sole periods used in this structural identification process.

5.1. Dynamic Body Compensation

In addition to the vibrational motion, there is the rigid body motion of the spacecraft due to the change in the ground observer's aspect angle. The apparent change has two effects on the observed Doppler shifted laser return.

1. The rigid body motion will be detected. This motion roughly approximates a mode with a low frequency. Thus the frequency separation between this apparent rigid body motion and the lowest vibrational mode of .019 Hz maybe very small. In order to detect the lowest mode, this apparent motion must be eliminated.
2. The observed damping factors of the detected modes will be affected by the position of the spacecraft in the sky. When the observation window is before the spacecraft comes overhead, the calculated damping factors will be smaller. If the modal frequency is small, the calculated damping factor could indeed become negative. Likewise, if the observation window is after the spacecraft goes overhead, the calculated damping factor will become larger than the true value.

The effects of this apparent motion are adjusted for.

5.2. Identification Analysis

The PSD of the data sets, sampled in-phase and quadrature,was filtered so as to detect the relative and vibrational motion of the spacecraft. The test data had Doppler shift measurements collected at a 62 Hz sample rate. This rate is significantly higher than the modes of interest. To filter out some of the noise present, groups of 5 samples are taken and the median value of the population is selected. This technique reduces the sample rate to 12.4 Hz, which is more than adequate for analysis. Reducing the sampling rate further was done with filtering and decimation in time.

Using this data, an initial analysis was performed. All the data was initially filtered to eliminate high noise components. Based on analysis of the detected motion PSD, the cutoff frequency was chosen to be .75 Hz. This number allows for decimation in time and is sufficiently separated from the higher modes. The data sets were then decimated in time into distinct data sets. Each of these data sets were then analyzed and statistically compared. (Note: The minimum model error results generated optimal data such that the variance between the actual and simulated data was approximately 1.8 mm/sec.

The results of this analysis are quite impressive. Given such short observation windows, the algorithms detected modes which correlate well with predictions. Four vibration modes were detected on day 91010, of which three were among the first four pitch plane vibration modes. Three vibration modes were detected on day 91008, of which two were among the first four pitch plane vibration modes. The lowest predicted pitch mode is detectable only when the rigid body motion is removed from the data of day 91010. Day 91008 observation window was only 25 seconds long and this observation was too short to collect enough data on the lowest mode (modal period is $\approx$ 50 seconds).

Both observation days detected a mode not previously predicted by either the PDE or FEM models. This moderately damped mode at $\approx$ .52 Hz is probably not due to the boom elements because the damping is too high. While the explanation for this mode is yet unknown it is believed to be due to either unmodeled behavior within the boom canisters or vibrations that are due to the cantilevered retro-reflector plate. Such elastic behavior would tend to be nonlinear and will have higher damping. The nonlinear vibration assumption is supported by the size of the damping factor for the .52 Hz mode. Its damping factor was between 5 and 11 percent. This level is significantly higher than the other modes. This difference may be attributed to the nonlinear behavior in either the boom canister or at the cantilevered retro-reflector plate.

The identified modes were within .005 to .01 Hz of the predicted modes depending on the identification technique compared. While this is impressive, the identification of the damping factors had a larger variance. Of the predicted modes that were identified, Tables 6 and 8 show that two of the three modes had damping of approximately one to two percent. This agrees well with experiments done on the ground. The damping factor for the lowest mode of .019 Hz, had the largest variance associated with it. This variance is due to the fact that the period of observation was very short in comparison to the period of the mode which causes the parameter identification to be more sensitive to noise. In the future, longer observation windows will provide enough information to get better damping calculations.

Table 5: Day91008 Identification Results: Modal Frequencies

Model Mode Hz.	ERA Hz.	std. dev. Hz.	ERA/MME Hz.	std. dev. Hz.
0.1298	0.1225	0.0005	0.1226	0.0005
0.3238	0.3245	0.0003	0.3248	0.0006
	0.5219	0.0025	0.5201	0.0030

Table 6: Day91008 Identification Results: Damping Factors

Model Mode	ERA %	std. dev.	ERA/MME %	std. dev.
0.1298	-0.1244	0.2489	-0.3518	0.3027
0.3238	1.4477	0.0410	1.1137	0.0473
	4.8917	0.2984	4.5929	0.2631

Table 7: Day91010 Identification Results: Modal Frequencies

Model Mode Hz.	ERA Hz.	std. dev. Hz.	ERA/MME Hz.	std. dev. Hz.
0.0191	0.0208	0.0033	0.0210	0.0020
0.1298	0.1244	0.0010	0.1245	0.0011
0.3238	0.3312	0.0009	0.3320	0.0008
	0.5115	0.0061	0.5120	0.0064

Table 8: Day91010 Identification Results: Damping Factors

Model Mode	ERA %	std. dev.	ERA/MME %	std. dev.
0.0191	1.8385	1.8277	1.3937	2.260
0.1298	2.3233	0.5182	2.1029	0.3007
0.3238	2.1114	0.2312	2.0058	0.2971
	10.4537	1.2157	10.7973	1.0233

6. Conclusions and Interpretations

Considering the brevity of the observation windows, the experiment was extremely successful. The experiment accomplished the following goals:

1. Structural modes were verified independently using the actual spacecraft in its true environment. Three of the first four modes were detected. These results are impressive compared to previous experiments, specifically, the 1985 Solar Array Flight Experiment (SAFE). The SAFE experiment, which was a two day experiment done on board the space shuttle, tested the modal properties of a deployed truss with an attached solar panel. The SAFE experiment only detected three modes.
2. Algorithmic approaches were tested with an actual experiment. Algorithms provided robust identification. The identified modes were tightly grouped and agreed with predicted modes. A variety of identification techniques were compared on simulated data. The Hankel operator technique performed better than any other approach, given the type of signal and the short length of observation.
3. A new laser application was verified. This experiment showed that laser tracking could be accomplished and provide data on which analysis could be performed. This approach offers alternative experimental approaches to structural identification for low orbit satellites.
4. A system engineering approach was applied to a complex problem, whose technological solution spanned many disciplines. A requirement analysis review showed the need for large space systems. Structural identification is a necessary component of on-station health monitoring and real time control algorithms.

This experiment was designed to show that low cost low-complexity on-board hardware combined with algorithmic analysis can implement the identification process and aid in the progression toward real-time identification and control.

References

[1] D.J. Mook, J.L. Junkins, Minimum Model Error Estimation for Poorly Modeled Dynamic Systems, *AIAA Journal of Guidance, Control, and Dynamics*, 11(4):365-375, May-June 1988.

[2] S.A. de Vries. Frequency domain analysis of models of flexible beams. Master's thesis, University of Groningen, 1988.

[3] D. Enns, *Model reduction for Control System Design*, Ph.D. thesis, Standford, University, 1984.

[4] Glover, K., All-optimal Hankel-norm approximations of Linear multivariable systems and their L_∞ error bounds, *International Journal of Control*, 39:1115-1193, 1984.

[5] J.N. Juang, R.S. Pappa, An Eigensystem Realization Algorithm (ERA) for Modal Parameter Identification and Model Reduction, *AIAA Journal of Guidance, Control, and Dynamics*, 8(5):620-627, Sept-Oct 1985.

[6] K. Glover, R. Curtain and J. Partington, Realisation and Approximation of Linear Infinite-Dimensional Systems with Error Bounds, *SIAM Journal of Control, and Optimiazation*, 26(4):863-898, July 1988.

[7] K.I. Schultz, Analysis of Narrowband IR LACE Measurements Acquired during GMT days 195 and 200, MIT Lincoln Laboratory Memo, August 1990.